ARTICLE

doi:10.1038/nature12188

Mitonuclear protein imbalance as a conserved longevity mechanism

Riekelt H. Houtkooper[1,2]*, Laurent Mouchiroud[1]*, Dongryeol Ryu[1], Norman Moullan[1], Elena Katsyuba[1], Graham Knott[3], Robert W. Williams[4] & Johan Auwerx[1]*

Longevity is regulated by a network of closely linked metabolic systems. We used a combination of mouse population genetics and RNA interference in *Caenorhabditis elegans* to identify mitochondrial ribosomal protein S5 (*Mrps5*) and other mitochondrial ribosomal proteins as metabolic and longevity regulators. MRP knockdown triggers mitonuclear protein imbalance, reducing mitochondrial respiration and activating the mitochondrial unfolded protein response. Specific antibiotics targeting mitochondrial translation and ethidium bromide (which impairs mitochondrial DNA transcription) pharmacologically mimic *mrp* knockdown and extend worm lifespan by inducing mitonuclear protein imbalance, a stoichiometric imbalance between nuclear and mitochondrially encoded proteins. This mechanism was also conserved in mammalian cells. In addition, resveratrol and rapamycin, longevity compounds acting on different molecular targets, similarly induced mitonuclear protein imbalance, the mitochondrial unfolded protein response and lifespan extension in *C. elegans*. Collectively these data demonstrate that *MRPs* represent an evolutionarily conserved protein family that ties the mitochondrial ribosome and mitonuclear protein imbalance to the mitochondrial unfolded protein response, an overarching longevity pathway across many species.

Longevity is coordinated by intersecting pathways, often converging on metabolic networks[1–4]. A key player in lifespan regulation is the mitochondrion. Over a thousand proteins encoded by nuclear DNA (nDNA) translocate to and function in mitochondria[5], in synchrony with 13 proteins encoded by the mitochondrial DNA (mtDNA) that require a separate translation machinery, including mitochondrial ribosomal proteins (MRPs)[6,7]. Many molecular studies of longevity have exploited simple organisms and loss- or gain-of-function mutations, but the complex connectedness of mitochondrial and metabolic longevity networks benefits from an integrative cross-species approach[2].

Here we pioneered such a strategy and used the BXD reference population of mice[2,8–10] to identify mitochondrial ribosomal protein S5 (*Mrps5*) and other members of the *MRP* family as longevity genes. In *C. elegans*, we confirmed this role of MRPs and demonstrated that they induce a stoichiometric imbalance between nDNA- and mtDNA-encoded oxidative phosphorylation proteins, hereafter termed 'mitonuclear protein imbalance', which activates the mitochondrial unfolded protein response (UPR^{mt}). Our conclusions were corroborated using specific antibiotics targeting bacterial/mitochondrial translation, and ethidium bromide, which inhibits mtDNA transcription. This mechanism is shared with pathways that induce mitonuclear protein imbalance from a nuclear perspective, such as the UPR^{mt} and lifespan enhancing effects of rapamycin and resveratrol. Our data hence tie mitochondrial translation and metabolism to natural lifespan regulation across species.

A QTL for mouse longevity

The BXD family consists of fully inbred progeny of a cross between C57BL/6J and DBA/2J mice, with a complexity that matches many human populations[11]. Both parental strains have been sequenced, enabling analysis of sequence variants linked to phenotypes[12]. We used new genomic and genetic resources to re-analyse longevity data for BXD lines[13] using forward and reverse genetic methods[9].

The forward strategy exploits longevity data and updated high-density single nucleotide polymorphism (SNP) genotypes[14] archived in http://www.GeneNetwork.org. As reported[13], lifespan of BXDs varies from ~365 days for the shortest lived strain to ~900 days for the longest lived strain (Fig. 1a). We remapped longevity using the new genotypes and detected one genome-wide significant locus on chromosome 2 with a peak at 124–129 Mb (Fig. 1b, log odds ratio (lod) = 4.0). Two additional loci, on chromosomes 4 and 7, were not significant, but suggestive (lod = 2.8 and 3.0, respectively). However, neither was suggestive after controlling for SNP rs6374387 on chromosome 2 using composite interval mapping.

The chromosome 2 locus contains ~70 genes (Supplementary Table 1), none of which were previously linked to longevity. To evaluate and rank candidates, we correlated lifespan with multiple gene expression data sets. Only three genes in the locus correlate strongly with lifespan (Fig. 1c, $P < 0.01$; Supplementary Fig. 1): solute carrier family 12 member 1 (*Slc12a1*), mitochondrial ribosomal protein S5 (*Mrps5*) and tubulin tyrosine ligase (*Ttl*). From the natural variation in expression of these genes, we deduced that 50% reduction of expression corresponds to a ~250 day lifespan difference.

Conservation of longevity in *C. elegans*

We identified Y37A1C.1/*nkcc-1*, E02A10.1/*mrps-5*, and F25C8.5/*ttll-9* as worm homologues of *Slc12a1*, *Mrps5* and *Ttl*, respectively. RNA interference (RNAi)-mediated knockdown of *nkcc-1* and *mrps-5*, but not of *ttll-9*, extended lifespan (Fig. 2a).

Next, we compared expression of *Mrps5* and other *Mrp* family members in a muscle microarray of ageing and caloric restriction in C57BL/6J (ref. 15). *Mrp* expression decreased with age, an effect rescued by

[1]Laboratory for Integrative and Systems Physiology, Ecole Polytechnique Fédérale de Lausanne, CH-1015 Lausanne, Switzerland. [2]Laboratory Genetic Metabolic Diseases, Academic Medical Center, 1105 AZ Amsterdam, The Netherlands. [3]BioEM Facility, Ecole Polytechnique Fédérale de Lausanne, CH-1015 Lausanne, Switzerland. [4]Department of Anatomy and Neurobiology and Center for Integrative and Translational Genomics, Memphis, Tennessee 38163, USA.
*These authors contributed equally to this work.

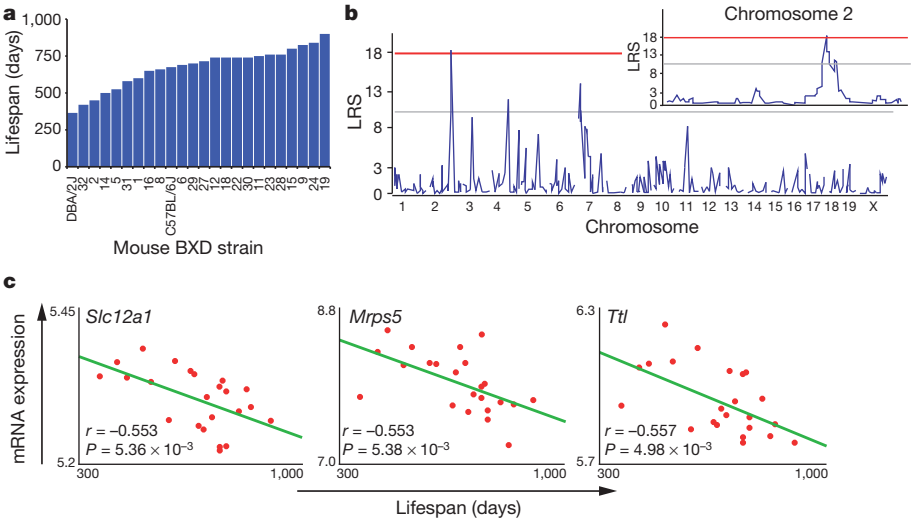

Figure 1 | Lifespan regulation in BXD recombinant inbred mice. **a**, Lifespan in different BXD strains. **b**, Interval mapping using the BXD lifespan data reveals a strong QTL on chromosome 2, between 124–129 Mb. The red line depicts the cut-off for statistical significance (P genome-wide <0.05), the grey line represents the limit for suggestive QTLs. See also Supplementary Table 1. LRS, likelihood ratio statistics. **c**, Pearson's r correlation coefficient with corresponding P values for the co-variation between BXD lifespan (x axis) and mRNA expression of the indicated gene in the BXD eye microarrays (y axis). Decreased expression of *Slc12a1*, *Mrps5* and *Ttl* robustly correlates with longevity ($P < 0.01$). Correlation coefficient trend line is shown in green.

caloric restriction; in contrast, expression of *Slc12a1* and *Ttl* was unaffected (Fig. 2b). Linkage of MRPs with lifespan is strengthened as many other *Mrp* family members also correlate with longevity (Fig. 2c). We extended our analyses to the DNA level using sequence data for *Mrps5* in both parental strains and identified missense variants in exon 3 (rs29667217 and rs13471334; V60A and V67I, respectively). Other sequence variants in *Mrps5* contribute to variation in transcript abundance; *Mrps5* mRNA levels among the BXDs are associated with a strong quantitative trait loci (QTL) superimposed over the gene itself—a cis-expression QTL.

Using a reverse genetics approach, we studied the *Mrps5*-associated network. *Mrps5* expression co-varies with genes involved in oxidative phosphorylation. Considering that oxidative metabolism is involved in known longevity pathways[2], the set of transcripts that co-vary with *Mrps5* qualified as an appealing longevity network. Oxidative phosphorylation was the most enriched network of *Mrps5* co-variates in both BXDs[16] and a conventional F2 intercross[17] ($P = 1.53 \times 10^{-21}$, $P = 5.78 \times 10^{-10}$, respectively). Finally, we generated an interaction network of oxidative phosphorylation genes with *Mrps5* (Fig. 2d), in which *Ndufb7* provides the hinge that links *Mrps5* to oxidative phosphorylation. Knockdown of the worm homologues for the network components *Ndufb7* and *Ndufa6* robustly extended lifespan[18–20]. *Mrps5* hence emerged as a strong longevity candidate, integrating protein synthesis and mitochondrial metabolism—both important longevity modulators.

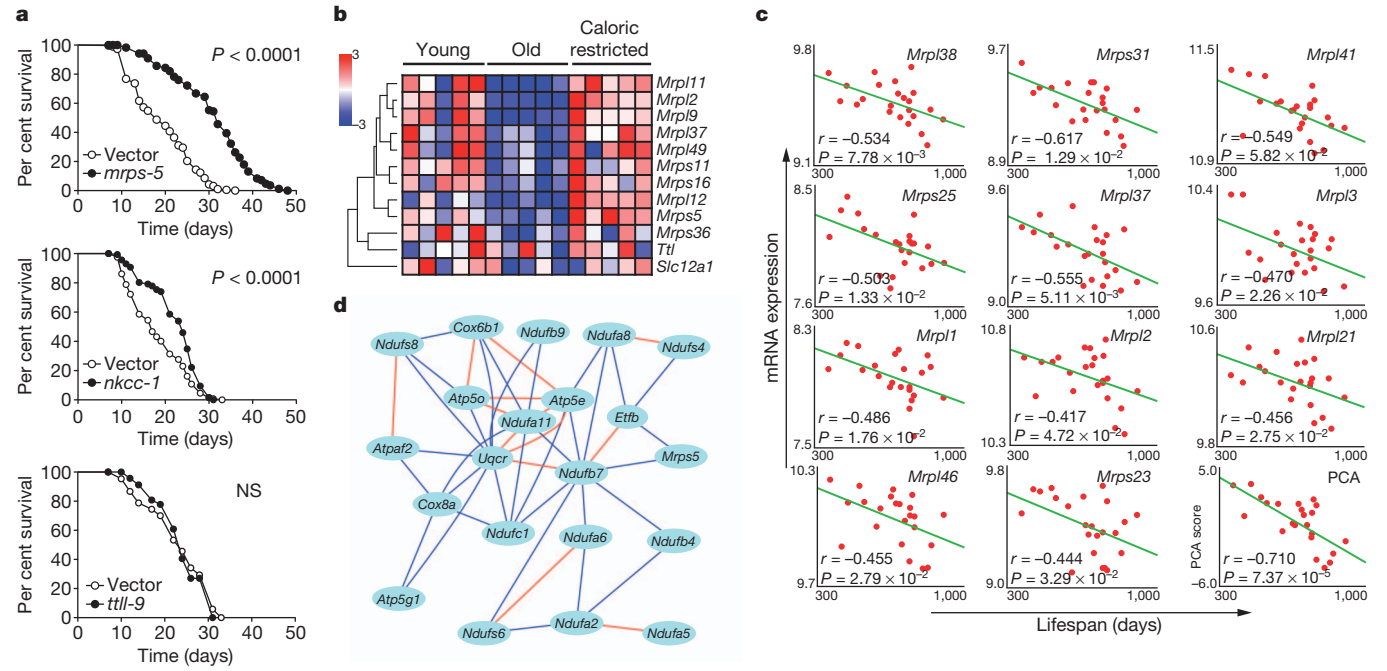

Figure 2 | Validation of *Mrps5* as a candidate longevity gene. **a**, Knockdown of *mrps-5*, *nkcc-1* or *ttll-9* throughout the entire life of *C. elegans* increased lifespan by 60%, 23% or 3%, respectively. See also Supplementary Table 2. NS, not significant. **b**, One-way hierarchical clustering showing gene expression differences in gastrocnemius muscle between young (5 months), old (25 months) and caloric restricted C57BL/6J mice[15]. Expression of mouse *Mrp* genes decreases upon ageing, and reverts with caloric restriction, whereas *Slc12a1* and *Ttl* do not change. The colour-coded heat map represents relative gene expression differences (red, large gene expression values; blue, small gene expression values). **c**, Pearson's r correlation coefficient with corresponding P values for co-variation between BXD lifespan (x axis) and mRNA expression of eleven other *Mrp* genes (y axis) indicates robust correlation. Principle component analysis (PCA) reveals a highly significant correlation between the *Mrp* gene family and BXD lifespan. **d**, *Mrps5* strongly correlates with genes involved in oxidative phosphorylation. Red lines indicate a positive Pearson correlation coefficient of 0.7–1.0, and blue lines indicate a correlation coefficient of 0.5–0.7.

Mitonuclear protein imbalance and ageing

To define causality of the *MRP*s in determining lifespan, we knocked down *mrp* genes during the entire life of the worm and robustly increased lifespan (Fig. 3a and Supplementary Table 2). Similar to well-characterized mitochondrial mutants that live longer, larval development was delayed (Supplementary Fig. 2a)[21]. Knockdown during development proved crucial and sufficient to extend lifespan, whereas RNAi during adulthood alone did not (Fig. 3b, Supplementary Fig. 2b and Supplementary Table 2), as reported in other long-lived mitochondrial mutants[22]. Increased lifespan was not due to effects on feeding, as pharyngeal pumping rates were normal (Supplementary Fig. 2c). *mrps-5* RNAi also delayed physiological decline with age. Even though they moved slightly less in early adulthood (day 3), *mrps-5* RNAi worms move twice as much as controls at day 13, and this effect becomes more pronounced at day 20 (Supplementary Fig. 2d, e and Supplementary Videos 1–4). This difference was accompanied by a delay in decline of pharyngeal pumping (Supplementary Fig. 2c) and in muscle fibre disorganization (Fig. 3c), hallmarks of fitness of aged *mrps-5* RNAi worms.

In line with the mitochondrial connection of *Mrps5*, basal respiration was reduced upon *mrp* knockdown and unresponsive to the mitochondrial uncoupler carbonyl cyanide *p*-trifluoromethoxyphenylhydrazone (FCCP) (Fig. 3d). As a consequence, *mrps-5* RNAi worms displayed reduced ATP levels and citrate synthase activity (Fig. 3e, f), indicative of reduced mitochondrial abundance or activity. Consistent with its role in mitochondrial translation, *mrps-5* RNAi induced a stoichiometric imbalance between nDNA- and mtDNA-encoded oxidative phosphorylation subunits, termed mitonuclear protein imbalance, visualized by selective reduction in MTCE.26 (MTCO-1 homologue; from mtDNA) relative to H28O16.1 (ATP5A homologue; from nDNA) expression (Fig. 3g). The mitonuclear protein imbalance and consequences for mitochondrial function was similar to the long-lived *cco-1* mutant—deficient for the nDNA-encoded worm homologue of complex IV, subunit Vb/COX4—but not observed in the short-lived complex II SDHC mutant *mev-1* (Fig. 3g). Furthermore, mitochondria had a more punctuate globular pattern instead of the regular reticular or tubular appearance in both muscle (Fig. 3h) and intestine, a finding confirmed by electron microscopy (Supplementary Fig. 3a, b).

To identify which 'longevity pathways'—insulin/IGF-1 signalling[23], caloric restriction[24] or mitochondrial dysfunction[22]—are required for the lifespan phenotype, we reduced *mrps-5* expression in worms carrying mutations in these pathways. *mrps-5* RNAi increases lifespan by ~40% in wild type (Fig. 3i), similar to the effect in *daf-2*, *daf-16*, *eat-2*, *sir-2.1* and *aak-2* mutants (Fig. 3j–l and Supplementary Fig. 4a–e) indicating that *mrps-5* regulates longevity independently of insulin/IGF-1 (*daf-16*/*daf-2*) and caloric restriction (*eat-2*/*sir-2.1*) and acts downstream of mitochondrial regulator *aak-2*.

We focused on the mitochondrial pathway, because (1) it robustly effects longevity[22]; (2) *MRP*s function in the translation of mtDNA-encoded oxidative phosphorylation subunits[6,7]; and (3) in the BXDs, *Mrps5* networked with several oxidative phosphorylation components (Fig. 2d). *mrps-5* RNAi reverts the short-lived phenotype of *mev-1* mutants, with a dramatic 112% lifespan extension (Fig. 3m and Supplementary Fig. 4f). *mrps-5* RNAi in the *cco-1* mutants did not extend lifespan compared to *mrps-5* RNAi alone, indicating that *cco-1* and *mrps-5* act in a similar fashion (Fig. 3n and Supplementary Fig. 4g). The same is true for *mrps-5* RNAi in the mitochondrial *clk-1*(*e2519*)

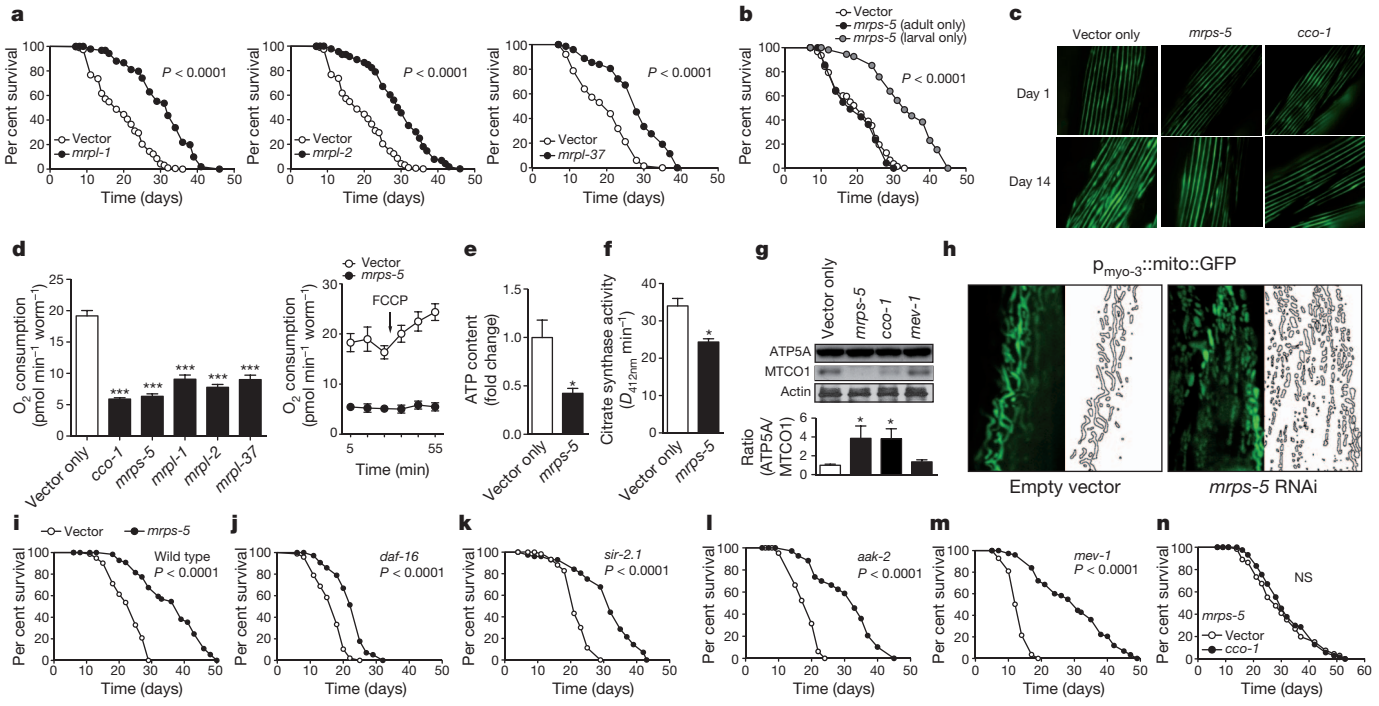

Figure 3 | *mrps-5* RNAi prevents ageing-associated functional decline and alters mitochondrial function. **a**, Knockdown of *mrpl-1*, *mrpl-2* or *mrpl-37* increased lifespan by 57%, 54%, or 41%, respectively. **b**, When RNAi of *mrps-5* was performed during the larval stages only, lifespan increased by 48%, whereas RNAi started from the L4 stage had no effect. $P \leq 0.001$ is for larval-only versus either vector control or adult-only. **c**, *mrps-5* or *cco-1* RNAi prevented age-related changes in muscle morphology as evidenced by a worm $p_{myo\text{-}3}$MYO-3::GFP reporter marking myosin heavy chain. **d**, *mrp* RNAi in *C. elegans* decreased respiration. Respiration per worm is shown, respiration was similarly decreased when corrected for protein. FCCP was added at the indicated time. Values are mean ± s.e.m. ($n = 10$), $^{***}P \leq 0.001$. **e–g**, *mrps-5* RNAi decreased ATP levels (**e**, $n = 3$), citrate synthase activity (**f**, $n = 3$), and altered the ratio between nDNA (ATP5A) versus mtDNA-encoded (MTCO1) oxidative phosphorylation proteins, similar to *cco-1*, but not *mev-1* (**g**, $n = 4$). $^{*}P \leq 0.05$. *A*, attenuance. **h**, *mrps-5* RNAi resulted in fragmented mitochondria, as visualized in body wall muscle (day 2, adult worms) using the $p_{myo\text{-}3}$::mito::GFP reporter, which expresses mitochondrial-targeted GFP driven by the muscle-specific *myo-3* promoter. **i**, *mrps-5* RNAi increased mean lifespan by 40%. **j–m**, *mrps-5* RNAi extends lifespan of *daf-16*(*mu86*) (**j**), *sir-2.1*(*ok434*) (**k**), *aak-2*(*ok524*) (**l**), *mev-1*(*kn1*) (**m**) mutants by 37%, 40%, 69% and 112%, respectively. **n**, Knockdown of *cco-1* does not extend lifespan of *mrps-5* RNAi worms. See Supplementary Table 2 and Fig. 4.

mutant, confirming the link with mitochondrial longevity pathways (Supplementary Fig. 4h).

Mitochondrial unfolded protein response

The mitochondrial unfolded protein response accounts for longevity upon *cco-1* loss-of-function and is selective for the mitochondrial pathway and not involved in the caloric restriction or insulin/IGF-1 pathways[25]. UPR^{mt} is induced by mitochondrial stress, subsequently activating a nuclear transcriptional response, inducing the chaperones HSP-6 (HSP-70 in mammals) and HSP-60 to restore mitochondrial proteostasis[26,27]. We monitored UPR^{mt} using *hsp-6*::GFP (green fluorescent protein) and *hsp-60*::GFP reporter worms with reduced *mrp* expression. Similar to the *cco-1* mutant[25], *hsp-6* and *hsp-60* were induced in worms with reduced *mrp* (Fig. 4a–c and Supplementary Fig. 5a, b). This was specific for UPR^{mt}, as *mrps-5* RNAi did not affect UPR in the endoplasmic reticulum (UPR^{ER}) and cytosolic heat shock response (Supplementary Fig. 5c). As for lifespan, UPR^{mt} was not induced when *mrp* expression was only inhibited during adulthood (Supplementary Fig. 5d). We measured UPR^{mt} upon combined *mrps-5* and *mev-1* inactivation. Whereas *mev-1* RNAi alone did not induce UPR^{mt} (Fig. 4c, d), combined inactivation induced mitonuclear protein imbalance (Supplementary Fig. 5e) and synergistically induced UPR^{mt} (Fig. 4d), accounting for the extended lifespan. Double inactivation of *mrps-5* and *cco-1* did not further enhance UPR^{mt} compared to *mrps-5* alone (Fig. 4d), in line with the similar lifespan.

There are individual differences in the degree of UPR^{mt} within the *mrps-5* RNAi worm population, which tightly correlate with lifespan extension (Supplementary Fig. 5f, h). GFP expression stayed similar throughout life, demonstrating that this is not an artefact of transiently reduced food intake (Supplementary Fig. 5i). To further link the level of UPR^{mt} to longevity, we measured UPR^{mt} in worms treated with RNAi against *mrp* genes[28]. Reduced expression of each *mrp* gene activated UPR^{mt} to a different degree (Supplementary Fig. 6a). The level of UPR^{mt} again correlated significantly with lifespan extension (Fig. 4e, Supplementary Fig. 6a, b and Supplementary Table 3).

Two downstream effectors of UPR^{mt} are HAF1, a mitochondrial peptide transporter[29], and UBL5, a ubiquitin-like protein that regulates the transcriptional activation of mitochondrial chaperones[30]. Knockdown of *haf-1* along with *mrps-5* RNAi reduced lifespan extension, UPR^{mt} and increased respiration (Fig. 4f–h). Similarly, when both *ubl-5* and *mrps-5* were knocked down, lifespan extension, the respiration phenotype and UPR^{mt} were partially lost, in line with the double *cco-1* and *ubl-5* RNAi treatment[25] (Supplementary Fig. 7a–f).

This network could be traced back to mice, as *Ubl5* and the most likely mouse *haf-1* homologue—*Abcb10*—correlated tightly with *Mrp* genes, for instance in the hippocampus of the BXDs[31] and in adipose tissue of F2-intercrossed mice[17] (Fig. 4i and Supplementary Fig. 7g). Additionally, *Hspd1* (also known as *Hsp60*) correlated with several *Mrp* genes (Fig. 4i and data not shown). Gene ontology analysis showed strong connectivity between *Ubl5* and oxidative phosphorylation genes ($P = 9 \times 10^{-4}$ in eye; $P = 8.62 \times 10^{-10}$ in hippocampus), the translation process or ribosome ($P = 6 \times 10^{-4}$ eye; $P = 6.03 \times 10^{-10}$ hippocampus) and the mitochondrial inner membrane ($P = 1 \times 10^{-4}$ eye; $P = 3.31 \times 10^{-27}$ hippocampus) in the BXDs. Finally, we tied *Hspd1* in a close correlation network with various *Mrp* and oxidative phosphorylation genes (Fig. 4j).

Pharmacological mitonuclear protein imbalance

Many mitochondrial functions can be traced back to their endosymbiotic 'bacterial' origin. Consequently, antibiotics that target bacterial translation also inhibit mitochondrial translation. We therefore used doxycycline to confirm the role of mitochondrial translation in longevity, using carbenicillin—targeting the bacterial cell wall—as a control. We used heat-killed OP50 or live HT115 bacteria—the latter insensitive to low concentrations of doxycycline (data not shown)—to feed worms, to prevent antibiotic effects on bacteria. Doxycycline, given throughout life, dose-dependently extended lifespan, induced UPR^{mt} not UPR^{ER}, and reduced oxygen consumption, without affecting ATP levels or citrate synthase activity (Fig. 5a–e and Supplementary Fig. 8a, b). Doxycycline at 60 μg ml^{-1} caused developmental

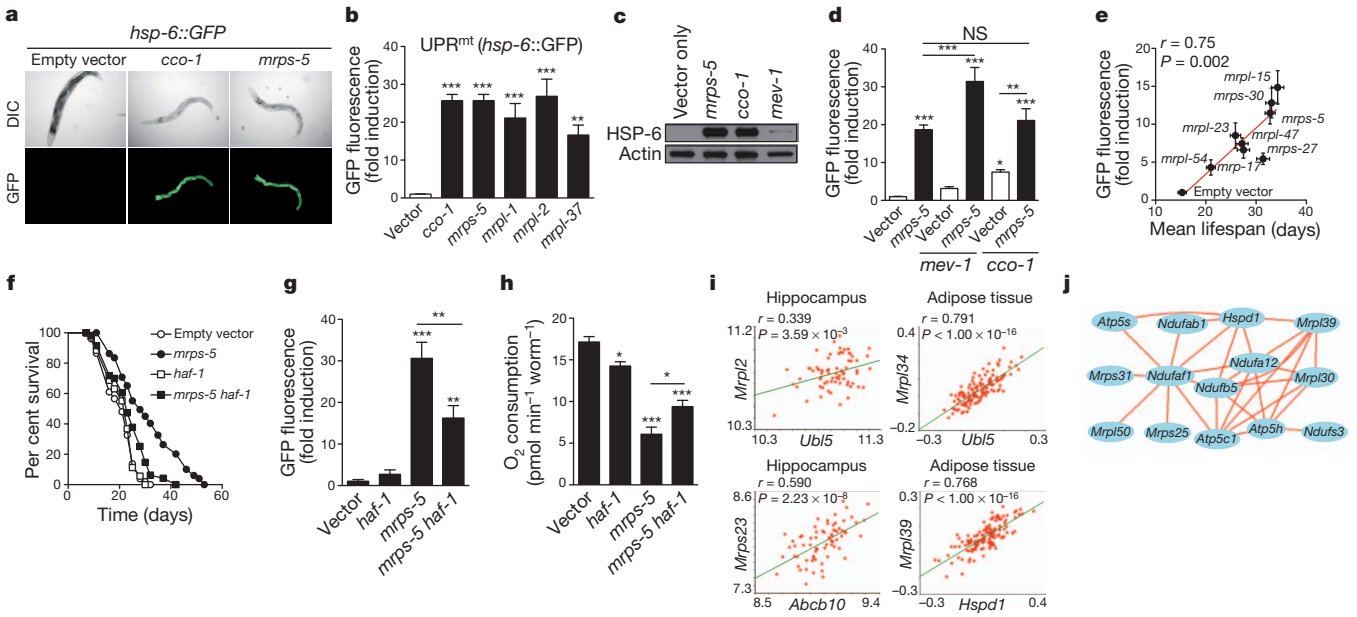

Figure 4 | *mrp* genes confer longevity effects through UPR^{mt}. **a**, RNAi of *mrp* genes induced UPR^{mt} (*hsp-6*::GFP reporter), similar to *cco-1* knockdown. Worms were synchronized at day 1 of adulthood. DIC, differential interference contrast. **b**, Quantification of UPR^{mt} upon knockdown of *mrp* or *cco-1* ($n = 4$). **c**, *mrps-5* and *cco-1*, but not *mev-1*, RNAi induce UPR^{mt} as reflected by the induction of HSP-6::GFP protein. **d**, Combined RNAi of *mrps-5* and *mev-1* synergistically increased UPR^{mt}, whereas combined *cco-1* and *mrps-5* RNAi did not further increase UPR^{mt} ($n = 6$). **e**, Knockdown of different *mrp* genes results in different levels of UPR^{mt}, which correlates with mean lifespan ($n = 33$–61 worms for lifespan, $n = 3$ for GFP). **f**–**h**, Epistasis with UPR^{mt} regulator *haf-1*. Double RNAi of *mrps-5* and *haf-1* partially prevented lifespan extension (**f**), UPR^{mt} (**g**, $n = 5$), and reduction in respiration (**h**, $n = 10$), compared to *mrps-5* RNAi alone. **i**, In various tissues of mouse crosses, *Ubl5*, *Abcb10* and *Hspd1* expression correlated with *Mrp* expression. **j**, *Hspd1* (also known as *Hsp60*) ties in a correlation network with *Mrp* and oxidative phosphorylation genes. Connecting lines indicate a Pearson correlation coefficient of 0.75–1.0. Bar graphs show mean ± s.e.m., $*P \leq 0.05$; $**P \leq 0.01$; $***P \leq 0.001$. See also Supplementary Figs 5–7 and Supplementary Table 3.

delay, like *mrps-5* RNAi, but no abnormalities were apparent at lower concentrations (data not shown). A low concentration of doxycycline (6 μg ml^{-1}), given only during development, also increased lifespan and UPR^{mt} and attenuated respiration (Fig. 5f–h). Chloramphenicol—belonging to a different class of antibiotics targeting translation—also increased lifespan and UPR^{mt}, at the same time as decreasing respiration (Fig. 5i–k), when administered during development. Similar to *mrps-5* RNAi, doxycycline increased the ratio of nDNA- (ATP5A) over mtDNA-encoded (MTCO1) oxidative phosphorylation proteins (Fig. 5l).

Linking back to mammals, doxycycline decreased respiration in a mouse hepatocyte cell line (Fig. 5m). Doxycycline also induced UPR^{mt}, as evidenced by induction of *Hsp60* (Fig. 5n) and the UPR^{mt} protease *ClpP* (Supplementary Fig. 8c), and increased HSP60 protein expression in hepatocyte cell lines and primary murine hepatocytes (Fig. 5o, p). Doxycycline induced a striking mitonuclear protein imbalance in hepatocytes (Fig. 5o, p). Finally, feeding mice with doxycycline for 10 days lowered oxygen consumption *in vivo*, indicative of attenuated mitochondrial function (Fig. 5q).

Similar effects on mitonuclear protein imbalance, UPR^{mt}, respiration and lifespan, without affecting mitochondrial morphology, were also observed in worms exposed to low concentrations of ethidium bromide, which inhibits mtDNA transcription specifically[32] (Supplementary Fig. 8d–h). This indicates that mitonuclear protein imbalance is the common underlying mechanism that links basic mitochondrial function to lifespan regulation.

A conserved longevity mechanism

To define how intricately mitonuclear protein imbalance and UPR^{mt} are involved in longevity, we analysed its activation in worms exposed to rapamycin[33,34]. Rapamycin inhibits TOR signalling to alter nDNA translation, inducing mitonuclear protein imbalance[35], and increases lifespan in various species, including mice[33]. Rapamycin also increased mean worm lifespan (by 16%)[34] in a *ubl-5*-dependent manner, induced UPR^{mt}, but not UPR^{ER} or heat shock response, and increased respiration (Fig. 6a, c and Supplementary Fig. 9a). This was associated with increased ATP levels, equal citrate synthase activity and altered nDNA/mtDNA oxidative phosphorylation protein ratio (Fig. 6d, e). Additionally, rapamycin changed the balance between nDNA- and mtDNA-encoded oxidative phosphorylation subunits in mouse hepatocytes in a dose dependent manner (Fig. 6f, g). This mitonuclear protein imbalance induced HSP60 and ClpP (Fig. 6f–h). Similarly, the lifespan enhancer resveratrol induced mitonuclear protein imbalance in hepatocytes (Fig. 6i) and *ubl-5*-dependently increased worm lifespan and UPR^{mt}, but not UPR^{ER} or heat shock response, at the same time as increasing respiration and maintaining ATP levels and citrate synthase activity (Supplementary Fig. 9b–f). Mitonuclear protein imbalance and UPR^{mt} hence represent an overarching mechanism of longevity that also can be engaged by pathways that signal mainly through the nucleus.

Finally, we tested whether reactive oxygen species (ROS) and mitohormesis, a theory which posits that an initial ROS burst (after 24 h) induces adaptive long-term protection[36], could explain our worm phenotypes. However, no ROS was produced after 24 h of *mrps-5* RNAi or doxycycline, rapamycin or ethidium bromide treatment (Supplementary Fig. 10a). In addition, the mitohormesis regulators *daf-16* and *aak-2* (ref. 36, 37) were not involved in UPR^{mt} induction (Supplementary Fig. 10b) or lifespan extension (Fig. 3j, l) following *mrps-5* RNAi. Finally, the ROS scavenger *N*-acetylcysteine (NAC) did

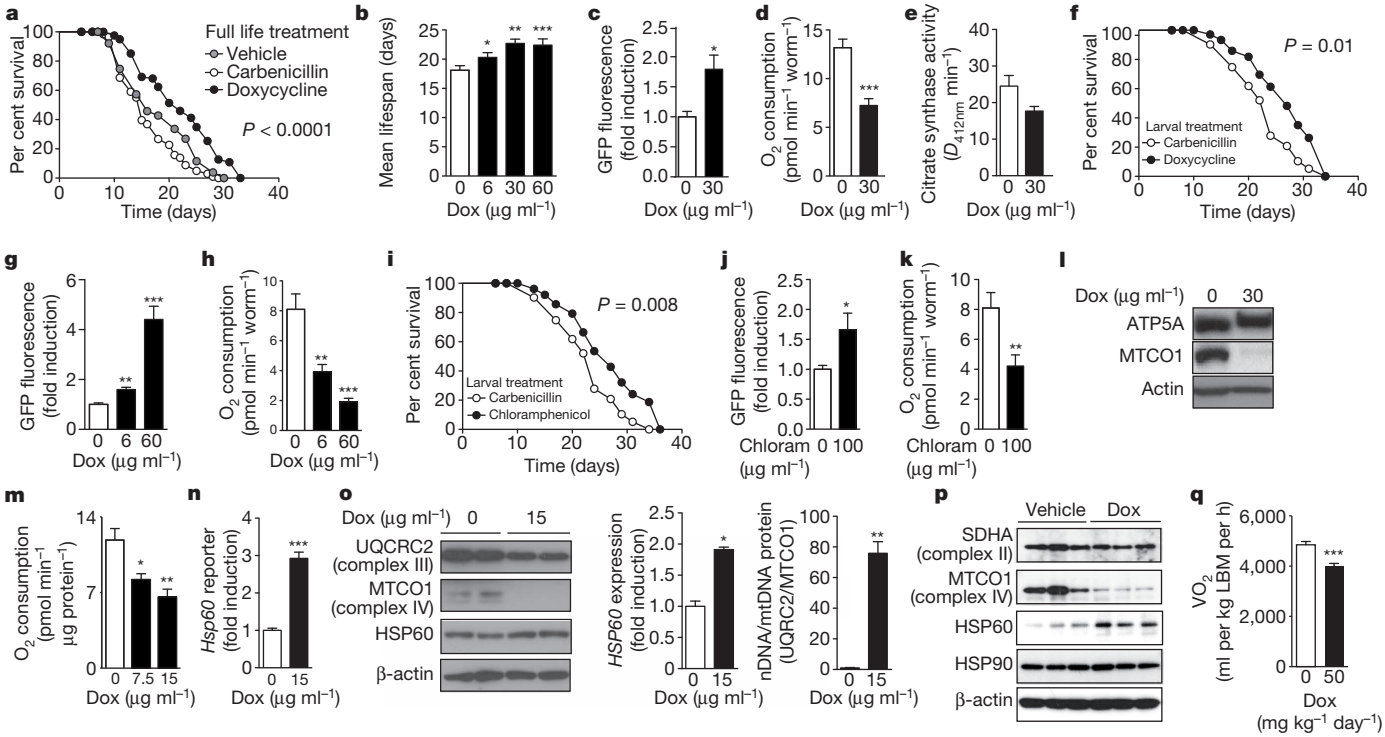

Figure 5 | Specific antibiotics extend lifespan by phenocopying *mrps-5* knockdown. **a**, Effects on worm lifespan of doxycycline (30 μg ml^{-1}), compared to carbenicillin (30 μg ml^{-1}) or vehicle. $P \leq 0.001$ refers to statistical significance of doxycycline compared to either vehicle or the carbenicillin control. Antibiotics were given throughout life in panels **a–e**. **b**, The effects of doxycycline (Dox) on lifespan are dose-dependent. **c–e**, Doxycycline induced UPR^{mt} (**c**, $n = 5$) and reduced respiration (**d**, $n = 10$), without changing citrate synthase activity (**e**, $n = 3$). **f–k**, When treated only during larval development, doxycycline (6 μg ml^{-1}, **f–h**) and chloramphenicol (Chloram, 100 μg ml^{-1}; **i–k**) extend lifespan (**f**, **i**), induced UPR^{mt} (**g**, **j**, $n = 5$) and reduced respiration (**h**, **k**, $n = 6$). **l**, Doxycycline alters the ratio between nDNA- (ATP5A) and mtDNA-encoded (MTCO1) oxidative phosphorylation proteins in worms. Doxycycline decreased respiration in a cultured hepatocyte cell line (**m**, $n = 5$), induced *Hsp60* transcription, as measured using an *Hsp60* promoter reporter (**n**, $n = 8$) and increased HSP60 protein expression and altered the ratio of nDNA- (UQCRC2) versus mtDNA- (MTCOI) encoded proteins (**o**, $n = 2$). **p**, Doxycycline increased HSP60 protein and altered the ratio of nDNA- versus mtDNA-encoded proteins in primary murine hepatocytes. **q**, Doxycycline (50 mg kg^{-1} day^{-1}) for 10 days in C57BL/6N mice decreased oxygen consumption ($n = 10$). LBM, lean body mass. See also Supplementary Table 2. *$P \leq 0.05$; **$P \leq 0.01$; ***$P \leq 0.001$.

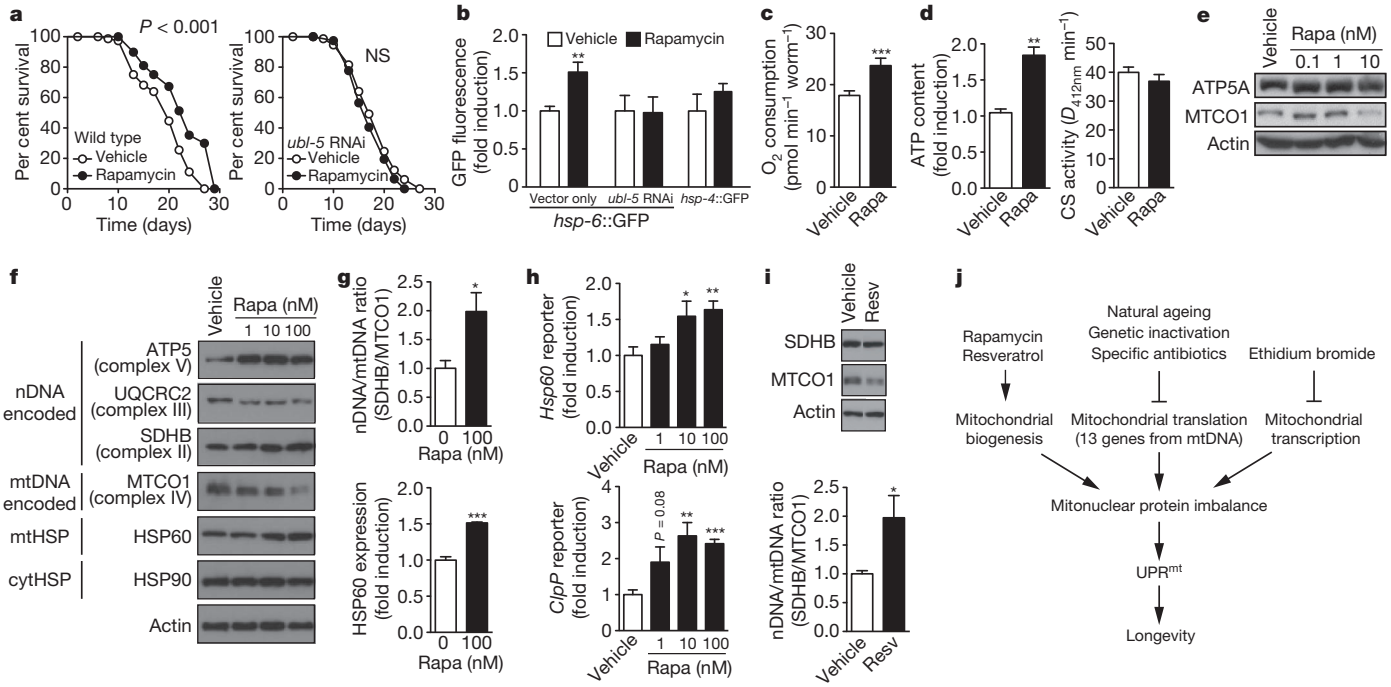

Figure 6 | Conserved function of mitonuclear protein imbalance and UPR^{mt} in longevity. **a**, Rapamycin (Rapa, 1 nM) extends worm lifespan in a *ubl-5*-dependent manner; **b**, *ubl-5*-dependently induced UPR^{mt} (*hsp-6*::GFP) but not UPR^{ER} (*hsp-4*::GFP) ($n = 4$). **c–e**, Rapamycin increased respiration (**c**, $n = 10$) and ATP content but not citrate synthase activity (**d**, $n = 3$) and induced mitonuclear protein imbalance (**e**). **f–h**, In mouse hepatocytes, rapamycin induces mitonuclear protein imbalance (**f**, **g**) and induces UPR^{mt} as shown at the protein (**f**, **g**, $n = 3$), and transcriptional (**h**, $n = 8$) level. **i**, Resveratrol (Resv, 25 μM) induced mitonuclear protein imbalance in mouse hepatocytes ($n = 4$). **j**, Hypothetical scheme of the mechanism by which reduced *Mrp* expression (during ageing or genetic inactivation), specific antibiotics, ethidium bromide and rapamycin and resveratrol extend lifespan by inducing UPR^{mt}. Bar graphs are shown as mean ± s.e.m., $*P \leq 0.05$; $**P \leq 0.01$; $***P \leq 0.001$. See also Supplementary Table 2.

not abrogate the *mrps-5* RNAi- or rapamycin-induced UPR^{mt}, nor did it suppress longevity (Supplementary Fig. 10c–f), similar to NAC-treated *cco-1* RNAi worms[25]. Together, these data demonstrate that, even though mitohormesis is important for insulin/IGF1-dependent ageing[37], UPR^{mt}-mediated longevity is independent of ROS.

Discussion

Using the BXD inbred wild type mouse panel, we identified a chromosome 2 QTL that is responsible for longevity, with *Slc12a1*, *Mrps5* and *Ttl* showing strong correlation with lifespan. A holistic approach, involving bioinformatics, genetics and pharmacological strategies in both worms and mammals, established that *Mrps5* and the *Mrp* protein family are the main actors in metabolic lifespan regulation. The MRPs constitute the mitoribosome that regulates translation of 13 mtDNA-encoded proteins, underscoring the vital importance of mitochondrial protein production[6,7].

Inhibiting mitochondrial translation reduced respiration and extended lifespan. There is an apparent dichotomy, however, as rapamycin (this study) as well as NAD$^+$ boosters—resveratrol (this study), nicotinamide riboside, nicotinamide and PARP inhibitors (L.M., R.H.H. and J.A., unpublished observations)—couple longevity to increased respiration. Abnormal mitochondrial proteostasis could reconcile these disparate observations. Knockdown of *mrps-5* or *cco-1* affect proteostasis and activate UPR^{mt} (refs 25, 28). From the *cco-1* study[25] it was, however, unclear if there was a direct connection between the level of UPR^{mt} and the lifespan extension. Our data demonstrate a positive correlation between the level of UPR^{mt} and lifespan. Moreover, UPR^{mt} seems to result from an imbalance between mtDNA- and nDNA-encoded proteins and is a common feature linking mitochondrial longevity pathways. Genetic defects in *mrp* or respiratory chain genes, antibiotics that inhibit translation, or moderate mtDNA transcription inhibition, induce such a mitonuclear protein imbalance from within mitochondria. Conversely, resveratrol and rapamycin change the production of nDNA-encoded mitochondrial proteins and if this is not matched with the levels of mtDNA-encoded proteins, mitonuclear protein imbalance and UPR^{mt} will also ensue, which favours longevity (Fig. 6j). The reason why *mev-1* mutants do not display UPR^{mt} is consistent with the fact that complex II is entirely nDNA-encoded and therefore does not require a balanced production of proteins from the nDNA and mtDNA. Additionally, complex II can be bypassed for mitochondrial ATP generation and is not part of oxidative phosphorylation supercomplexes[38]. Although further work to validate this hypothesis is warranted, this could explain apparent contradictions such as why mutations that either decrease or increase respiration can both induce longevity.

Our data identify MRPs as a novel longevity protein family, conserved from worms to mammals. The identification of these genes was triggered by analysis of murine reference populations. Hence, it is natural variation in *Mrp* expression, not artificial loss- or gain-of-function, that translates to longevity. In worms, longevity involves enhanced fitness and UPR^{mt}, and correlates tightly with levels of *mrp* knockdown. Our data suggest that stoichiometric imbalance between nDNA- and mtDNA-encoded oxidative phosphorylation proteins, or mitonuclear protein imbalance, is at the core of UPR^{mt} activation, both in worms and mammals. The apparent conservation of mitonuclear protein imbalance and UPR^{mt} as a general longevity mechanism should invite further studies to explore whether targeting UPR^{mt} can prevent ageing-associated functional decline and treat diseases linked with ageing.

METHODS SUMMARY

For the identification of novel longevity genes we used publicly available longevity data of the BXD genetic reference population. We used interval mapping in GeneNetwork (http://www.genenetwork.org; Trait ID 10112) for QTL analysis. Pearson's *r* genetic correlation was performed to establish genetic correlations with longevity. Candidate longevity genes were knocked down in wild type *C. elegans* strain Bristol N2, which were tested for lifespan at 20 °C. Worm UPR^{mt} was measured in the *hsp-6*::GFP or *hsp-60*::GFP reporter strains, and additional

mechanistic information was obtained after knockdown in other worm strains, as described in the online Methods. Treatments with carbenicillin, doxycycline, chloramphenicol, ethidium bromide, *N*-acetylcysteine, resveratrol and rapamycin (all from Sigma) were performed with heat-killed bacteria or with HT115 bacteria. Oxygen consumption in worms was measured using the Seahorse XF24 (Seahorse Bioscience) using 50 worms per well.

Mouse hepatocyte cell lines AML-12 or Hepa1-6, or primary mouse hepatocytes were used for mammalian conservation assays. UPR^{mt} was measured using luciferase reporters containing human *Hsp60* and *ClpP* promoter fragments and cellular oxygen consumption was measured using the Seahorse XF24 equipment. Mouse indirect calorimetry was performed in wild type C57BL/6N mice treated for 10 days with 50 mg kg^{-1} day^{-1} doxycycline as a food admix.

Full Methods and any associated references are available in the online version of the paper.

Received 15 May 2012; accepted 15 April 2013.

1. Fontana, L., Partridge, L. & Longo, V. D. Extending healthy life span–from yeast to humans. *Science* **328,** 321–326 (2010).
2. Houtkooper, R. H., Williams, R. W. & Auwerx, J. Metabolic networks of longevity. *Cell* **142,** 9–14 (2010).
3. Kenyon, C. J. The genetics of ageing. *Nature* **464,** 504–512 (2010).
4. Mair, W. & Dillin, A. Aging and survival: the genetics of life span extension by dietary restriction. *Annu. Rev. Biochem.* **77,** 727–754 (2008).
5. Pagliarini, D. J. *et al.* A mitochondrial protein compendium elucidates complex I disease biology. *Cell* **134,** 112–123 (2008).
6. Sharma, M. R. *et al.* Structure of the mammalian mitochondrial ribosome reveals an expanded functional role for its component proteins. *Cell* **115,** 97–108 (2003).
7. Anderson, S. *et al.* Sequence and organization of the human mitochondrial genome. *Nature* **290,** 457–465 (1981).
8. Liao, C. Y., Rikke, B. A., Johnson, T. E., Diaz, V. & Nelson, J. F. Genetic variation in the murine lifespan response to dietary restriction: from life extension to life shortening. *Aging Cell* **9,** 92–95 (2010).
9. Argmann, C. A., Chambon, P. & Auwerx, J. Mouse phenogenomics: the fast track to ''systems metabolism''. *Cell Metab.* **2,** 349–360 (2005).
10. Andreux, P. A. *et al.* Systems genetics of metabolism: the use of the BXD murine reference panel for multiscalar integration of traits. *Cell* **150,** 1287–1299 (2012).
11. Peirce, J. L., Lu, L., Gu, J., Silver, L. M. & Williams, R. W. A new set of BXD recombinant inbred lines from advanced intercross populations in mice. *BMC Genet.* **5,** 7 (2004).
12. Keane, T. M. *et al.* Mouse genomic variation and its effect on phenotypes and gene regulation. *Nature* **477,** 289–294 (2011).
13. De Haan, G. & Van Zant, G. Genetic analysis of hemopoietic cell cycling in mice suggests its involvement in organismal life span. *FASEB J.* **13,** 707–713 (1999).
14. Shifman, S. *et al.* A high-resolution single nucleotide polymorphism genetic map of the mouse genome. *PLoS Biol.* **4,** e395 (2006).
15. Edwards, M. G. *et al.* Gene expression profiling of aging reveals activation of a p53-mediated transcriptional program. *BMC Genomics* **8,** 80 (2007).
16. Geisert, E. E. *et al.* Gene expression in the mouse eye: an online resource for genetics using 103 strains of mice. *Mol. Vis.* **15,** 1730–1763 (2009).
17. Chen, Y. *et al.* Variations in DNA elucidate molecular networks that cause disease. *Nature* **452,** 429–435 (2008).
18. Lee, S. S. *et al.* A systematic RNAi screen identifies a critical role for mitochondria in *C. elegans* longevity. *Nature Genet.* **33,** 40–48 (2003).
19. Hamilton, B. *et al.* A systematic RNAi screen for longevity genes in *C. elegans*. *Genes Dev.* **19,** 1544–1555 (2005).
20. Hansen, M., Hsu, A. L., Dillin, A. & Kenyon, C. New genes tied to endocrine, metabolic, and dietary regulation of lifespan from a *Caenorhabditis elegans* genomic RNAi screen. *PLoS Genet.* **1,** e17 (2005).
21. Wong, A., Boutis, P. & Hekimi, S. Mutations in the *clk-1* gene of *Caenorhabditis elegans* affect developmental and behavioral timing. *Genetics* **139,** 1247–1259 (1995).
22. Dillin, A. *et al.* Rates of behavior and aging specified by mitochondrial function during development. *Science* **298,** 2398–2401 (2002).
23. Kenyon, C., Chang, J., Gensch, E., Rudner, A. & Tabtiang, R. A. *C. elegans* mutant that lives twice as long as wild type. *Nature* **366,** 461–464 (1993).
24. Lakowski, B. & Hekimi, S. The genetics of caloric restriction in *Caenorhabditis elegans*. *Proc. Natl Acad. Sci. USA* **95,** 13091–13096 (1998).
25. Durieux, J., Wolff, S. & Dillin, A. The cell-non-autonomous nature of electron transport chain-mediated longevity. *Cell* **144,** 79–91 (2011).
26. Haynes, C. M. & Ron, D. The mitochondrial UPR - protecting organelle protein homeostasis. *J. Cell Sci.* **123,** 3849–3855 (2010).
27. Zhao, Q. *et al.* A mitochondrial specific stress response in mammalian cells. *EMBO J.* **21,** 4411–4419 (2002).
28. Yoneda, T. *et al.* Compartment-specific perturbation of protein handling activates genes encoding mitochondrial chaperones. *J. Cell Sci.* **117,** 4055–4066 (2004).
29. Haynes, C. M., Yang, Y., Blais, S. P., Neubert, T. A. & Ron, D. The matrix peptide exporter HAF-1 signals a mitochondrial UPR by activating the transcription factor ZC376.7 in *C. elegans*. *Mol. Cell* **37,** 529–540 (2010).
30. Benedetti, C., Haynes, C. M., Yang, Y., Harding, H. P. & Ron, D. Ubiquitin-like protein 5 positively regulates chaperone gene expression in the mitochondrial unfolded protein response. *Genetics* **174,** 229–239 (2006).
31. Overall, R. W. *et al.* Genetics of the hippocampal transcriptome in mouse: a systematic survey and online neurogenomics resource. *Front. Neurosci.* **3,** 55 (2009).
32. Zylbee, E., Vesco, C. & Penman, S. Selective inhibition of the synthesis of mitochondria-associated RNA by ethidium bromide. *J. Mol. Biol.* **44,** 195–204 (1969).
33. Harrison, D. E. *et al.* Rapamycin fed late in life extends lifespan in genetically heterogeneous mice. *Nature* **460,** 392–395 (2009).
34. Robida-Stubbs, S. *et al.* TOR signaling and rapamycin influence longevity by regulating SKN-1/Nrf and DAF-16/FoxO. *Cell Metab.* **15,** 713–724 (2012).
35. Zid, B. M. *et al.* 4E-BP extends lifespan upon dietary restriction by enhancing mitochondrial activity in *Drosophila*. *Cell* **139,** 149–160 (2009).
36. Schulz, T. J. *et al.* Glucose restriction extends *Caenorhabditis elegans* life span by inducing mitochondrial respiration and increasing oxidative stress. *Cell Metab.* **6,** 280–293 (2007).
37. Zarse, K. *et al.* Impaired insulin/IGF1 signaling extends life span by promoting mitochondrial L-proline catabolism to induce a transient ROS signal. *Cell Metab.* **15,** 451–465 (2012).
38. Schägger, H. & Pfeiffer, K. Supercomplexes in the respiratory chains of yeast and mammalian mitochondria. *EMBO J.* **19,** 1777–1783 (2000).

Supplementary Information is available in the online version of the paper.

Acknowledgements We thank P. Gönczy and the *Caenorhabditis* Genetics Center for sharing or providing reagents. R.H.H. is supported by fellowships from NWO-Rubicon and AMC, and L.M. by an FRM fellowship. J.A. is the Nestlé Chair in Energy Metabolism and supported by EPFL, ERC (2008-AdG-23138), Velux Stiftung and SNSF. R.W.W. and GeneNetwork are supported by the National Institutes of Health (NIH) (P20-DA 21131, U01AA13499 and U01AA14425), and the UT Center for Integrative and Translational Genomics. R.W.W. and J.A. are supported by NIH grant R01AG043930.

Author Contributions D.R., N.M. and E.K. contributed equally to this work. R.H.H., L.M. and J.A. conceived and designed the project. R.H.H. and R.W.W. performed QTL mapping and sequence analyses. R.H.H., L.M., E.K., D.R., N.M., G.K. performed experiments. R.H.H. and J.A. wrote the manuscript with contributions from all other authors.

Author Information Reprints and permissions information is available at www.nature.com/reprints. The authors declare no competing financial interests. Readers are welcome to comment on the online version of the paper. Correspondence and requests for materials should be addressed to J.A. (admin.auwerx@epfl.ch).

METHODS

Forward genetics. For the *in silico* search for longevity genes, we have used publicly available longevity data of the BXD genetic reference population[39]. We used interval mapping in GeneNetwork (http://www.genenetwork.org), Trait ID 10112 for QTL analysis. Pearson's *r* genetic correlation was performed to establish genetic correlations with longevity (Eye M430v2 Data Set (Sept08) RMA)[40]. Principle component analysis (PCA) was performed using tools implemented in GeneNetwork.

Reverse genetics. We used BXD mice (Trait ID 1448488_at from Eye M430v2 (Sep08) RMA) and an F2 cross (Trait ID 10024407239 from UCLA BHF2 Adipose (June05) mlratio)[41] to analyse *Mrps5* correlates. We primarily used microarray data from the eye of BXD mice, as this organ contains multiple tissues and cell types—for example, neuronal and muscle—and because this microarray is very well annotated. We analysed correlates as follows: we selected the top 250 *Mrps5* correlates in both databases and performed Kyoto encyclopedia of genes and genomes (KEGG) and gene ontology analysis. For the network approach, we selected the oxidative phosphorylation genes within the top 250 traits associated with *Mrps5* and used the Pearson correlation coefficients to create a network (threshold = 0.6). For *Ubl5* and *Hspd1* correlates, we used a BXD hippocampus database[31], and adipose tissue data from an F2 intercross[41]. The *Hspd1* network was generated by selecting the oxidative phosphorylation and *Mrp* genes in the top 500 correlates in the F2 intercross adipose tissue (threshold = 0.75).

Hierarchical clustering. Unsupervised hierarchical clustering was performed using complete linkage and Pearson rank correlation distance on the *z*-score normalized gene expression data using software implemented in GenePattern[42,43].

***C. elegans* strains and RNAi experiments.** Strains used were wild-type Bristol N2, CB1370 *daf-2*(*e1370*) III, CB4876 *clk-1*(*e2519*) III, CF1038 *daf-16*(*mu86*) I, DA465 *eat-2*(*ad465*) II, RB754 *aak-2*(*ok524*) X, VC199 *sir-2.1*(*ok434*) IV, TK22 *mev-1*(*kn1*) III, SJ4100 (zcIs13[*hsp-6*::GFP]), SJ4058 (zcIs9[*hsp-60*::GFP]), SJ4005 (zcIs4[*hsp-4*::GFP]), SJ4103 (zcIs14*myo-3*::GFP(mit)]), SJ4143 (zcIs17*ges-1*::GFP(mit)]), RW1596 stEx30[*myo-3*p::GFP +*rol-6*(su1006)], and CL2070 (dvIs[*hsp-16.2*::GFP]). Strains were provided by the *Caenorhabditis* Genetics Center (University of Minnesota).

Bacterial feeding RNAi experiments were carried out as described[44]. Clones used were *mrps-5* (E02A10.1), *mrpl-1* (F33D4.5), *mrpl-2* (F56B3.8), *mrpl-37* (Y48E1B.5), *cco-1* (F26E4.9), *nkcc-1* (Y37A1C.1), *ubl-5* (F46F11.4), *haf-1* (C30H6.6), *mev-1* (T07C4.7), *mrp-17* (R12E2.12), *mrpl-47* (B0261.4), *mrpl-23* (T08B2.8), *mrpl-54* (F25H5.6), *mrps-30* (B0511.8), *mrps-27* (K11B4.1) and *mrpl-15* (Y92H12BR.8). Clones were purchased from GeneService and sequenced and RNAi clone information is shown in Supplementary Table 4. Double RNAi experiments were carried out by mixing the bacterial cultures directly before seeding on NGM plates. Controls were RNAi clones 50% diluted with control empty vector RNAi bacteria.

Lifespan tests were performed at 20 °C as described[45]. Treatments with carbenicillin, doxycycline, chloramphenicol, ethidium bromide, *N*-acetylcysteine, resveratrol and rapamycin (all from Sigma) were performed with heat-killed bacteria[46] or with HT115 bacteria.

Construction of *ttll-9* RNAi clones. The RNAi clone was cloned by reverse transcription PCR amplification of the corresponding cDNA from total RNA with following primers: *ttll-9*-XbaI (601–960): 5′-GGGTCTAGATCATAGCC ATACAGCTCGAAACAGTGGTTATCT-3′, *ttll-9*-KpnI (601–960): 5′-GGGG GTACCAAGTTCGATGTCAGAATCTATGTGCTGGTT-3′. PCR products were digested with KpnI/XbaI, and ligated into appropriately digested plasmid L4440.

Microscopy and GFP analysis. GFP expression and quantification were carried out as described[47]. Briefly, eighty worms (day 1 adults) were picked (20 per well of a black-walled 96-well plate) and GFP was monitored on a Victor X4 plate reader (Perkin Elmer). Each experiment was repeated at least twice. For picture acquisition of *hsp-6*::GFP expression, animals were mounted on 2% agarose pads in 10 mM tetramisole (Sigma) and examined using a Zeiss Axioplan-2 microscope (Carl Zeiss). Time lapse was performed by recording 10 pictures of mobile worms with a 10 s interval. Worm tracking was carried out using ImageJ software. Experiments were conducted with three worms from different plates.

Confocal microscopy and image processing. Worms were immobilized with tetramisole (Sigma) and mounted on 6% agarose pads on glass slides. Images were acquired using Zeiss LSM 700 upright confocal microscope (Carl Zeiss). For each condition, several worms were imaged. Image processing was performed with Fiji software. Tracing of the mitochondrial network contour was done by the use of Gaussian blur filter followed by the application of Laplacian operator.

Worm respiration assays. Oxygen consumption was measured using the Seahorse XF24 (Seahorse Bioscience). Typically, 200 animals were recovered from NGM plates with M9 medium, washed three times to eliminate residual bacteria, and resuspended in 500 µl M9 medium. Worms were transferred in 24-well Seahorse plates (50 worms per well) and oxygen consumption was measured 6 times. FCCP treatment was performed at 10 µM final concentration.

MitoSox staining. MitoSox staining was performed as previously described with slight modification[48]. Briefly, a population of 100 worms was recovered in 1 ml of M9 buffer, washed three times to remove residual bacteria, and resuspended in 200 µl of 1:200 MitoSox stock solution (initial stock solution was dissolved at 1 mM in dimethylsulphoxide (DMSO)). After 20 min of treatment, worms were washed five times in 1 ml of M9 buffer to eliminate the MitoSox reagent and then transferred in a black-walled 96-well plate for reading.

Quantification of ATP levels and citrate synthase enzymatic activity. Total ATP content was measured by the CellTiter-Glo luminescent cell viability assay (Promega). The luminescence was recorded with a Victor X4 plate reader (PerkinElmer) and values normalized by the total protein concentration determined using a Bradford assay.

Citrate synthase enzymatic activity was determined using the CS assay kit (Sigma). Absorbance at 412 nm was recorded on a Victor X4 (PerkinElmer) with 10 readings over the 1.5 min timespan. These readings were in the linear range of enzymatic activity. The difference between baseline and oxaloacetate-treated samples was obtained and used to calculate total citrate synthase activity according to the formula provided in the manual.

Worm electron microscopy. Worms were fixed using high pressure freezing (Leica Micosystems, HPM100) in low melting point agarose, freeze substituted in 0.5% osmium tetroxide, and 0.5% uranyl acetate in acetone at −90 °C, and then slowly warmed to −10 °C and transferred to pure acetone. Worms were embedded in increasing concentrations of epon resin at 20 °C, transferred to flat embedding moulds in pure resin, and cured at 65 °C for 48 h. Serial sections were cut at 50 nm, and placed onto formvar support films on single slot copper grids. These were imaged at 80 kV filament tension in a transmission electron microscope with a charge coupled device (CCD) camera (Tecnai Spirit, FEI Company, with Eagle 4k × 4k CCD camera).

Hsp60 and ClpP reporter assays. Human *HSPD1* (also known as *Hsp60*) and *CLPP* promoter fragments (−603 to +735 for *Hsp60*, and −1272 to +337 for *CLPP*) were amplified and ligated into the pGL3 basic vector (Promega). Primers used were HSP60-forward (5′-GACAACGCGTAACAAAAGAGGGGCGTCAG-3′) and HSP60-reverse (5′-GACACTCGAGCCCTGAGAAACCAAGTCAGC-3′), and ClpP-forward (5′-GACAACGCGT CTTTCCGGTCTGATCTCCAG-3′) and ClpP-reverse (5′-GACACTCGAGGTACCGTCTGCTCCACCAC-3′). The primers were tailed with MluI site (forward) and XhoI site (reverse).

The mouse hepatocyte cell line AML-12 (alpha mouse liver 12) was obtained from ATCC (Manassas). Cells were grown according to the supplier guidelines but in the absence of antibiotics unless specified.

Transfections were performed in 96-well plates using jetPEI (PolyPlus). Each well contained 30 ng of luciferase reporter and 5 ng of β-galactosidase expression plasmid. After 6 h of incubation with the DNA–jetPEI complexes, the transfection medium was exchanged for medium with or without doxycycline. Doxycycline was dissolved in DMSO and added to the cells in the medium.

Luciferase activity was measured with the luciferase assay system (Promega) in the Victor X4 (PerkinElmer) and normalized to β-galactosidase activity.

Cell culture and oxygen consumption. Hepa1-6 mouse liver cells were maintained in DMEM medium containing 4.5 g per litre glucose and 10% fetal calf serum. Hepa1-6 cells were incubated for 48 h with doxycycline or chloramphenicol (both Sigma) in medium containing 1 g per litre glucose, with 1% (v/v) oleate-BSA (Sigma) supplementation, and without any other antibiotics. Oxygen consumption was measured using the Seahorse XF24 equipment[49], and normalized for protein content.

Mouse indirect calorimetry. Wild type C57BL/6N mice were treated for 10 days with 50 mg kg^{-1} day^{-1} doxycycline (Sigma) as a food admix. Oxygen consumption (VO_2) was monitored by indirect calorimetry using the comprehensive laboratory animal monitoring system (CLAMS) (Columbus Instruments)[50].

Culture of primary hepatocytes. Primary hepatocytes were prepared from 8–10-week-old C57BL/6 mice by collagenase perfusion method as described[51,52]. Isolated primary hepatocytes were plated with medium 199 (Gibco) including 10% FCS, 10 units per ml penicillin and 10 µg ml^{-1} streptomycin. After 3–6 h attachment, cells were replaced with media without FCS and treated with 30 µg ml^{-1} doxycycline or DMSO every 24 h. Primary hepatocytes were harvested 48 h later.

Western blotting. Western blotting was performed with antibodies against HSP60 (N-20), HSP90 (BD Transduction Laboratories), β-actin (Santa Cruz Biotechnology), MitoProfile Total OXPHOS Rodent WB Antibody Cocktail against ATP5A (H28O16.1 in worms), MTCO1/COX1 (MTCE.26 in worms) and UQCRC2 (Abcam), green fluorescent protein (Cell Signaling) HRP-labelled anti-goat and anti-mouse secondary antibodies.

39. De Haan, G. & Van Zant, G. Genetic analysis of hemopoietic cell cycling in mice suggests its involvement in organismal life span. *FASEB J.* **13,** 707–713 (1999).

40. Geisert, E. E. *et al.* Gene expression in the mouse eye: an online resource for genetics using 103 strains of mice. *Mol. Vis.* **15,** 1730–1763 (2009).
41. Chen, Y. *et al.* Variations in DNA elucidate molecular networks that cause disease. *Nature* **452,** 429–435 (2008).
42. Reich, M. *et al.* GenePattern 2.0. *Nature Genet.* **38,** 500–501 (2006).
43. de Hoon, M. J., Imoto, S., Nolan, J. & Miyano, S. Open source clustering software. *Bioinformatics* **20,** 1453–1454 (2004).
44. Kamath, R. S., Martinez-Campos, M., Zipperlen, P., Fraser, A. G. & Ahringer, J. Effectiveness of specific RNA-mediated interference through ingested double-stranded RNA in *Caenorhabditis elegans*. *Genome Biol.* **2,** research0002—research0002.10 (2000).
45. Mouchiroud, L. *et al.* Pyruvate imbalance mediates metabolic reprogramming and mimics lifespan extension by dietary restriction in *Caenorhabditis elegans*. *Aging Cell* **10,** 39–54 (2011).
46. Wood, J. G. *et al.* Sirtuin activators mimic caloric restriction and delay ageing in metazoans. *Nature* **430,** 686–689 (2004).
47. Durieux, J., Wolff, S. & Dillin, A. The cell-non-autonomous nature of electron transport chain-mediated longevity. *Cell* **144,** 79–91 (2011).
48. Yang, W. & Hekimi, S. A mitochondrial superoxide signal triggers increased longevity in *Caenorhabditis elegans*. *PLoS Biol.* **8,** e1000556 (2010).
49. Watanabe, M. *et al.* Bile acids induce energy expenditure by promoting intracellular thyroid hormone activation. *Nature* **439,** 484–489 (2006).
50. Lagouge, M. *et al.* Resveratrol improves mitochondrial function and protects against metabolic disease by activating SIRT1 and PGC-1α. *Cell* **127,** 1109–1122 (2006).
51. Ryu, D. *et al.* Endoplasmic reticulum stress promotes LIPIN2-dependent hepatic insulin resistance. *Diabetes* **60,** 1072–1081 (2011).
52. Noriega, L. G. *et al.* CREB and ChREBP oppositely regulate SIRT1 expression in response to energy availability. *EMBO Rep.* **12,** 1069–1076 (2011).